



HAL
open science

Impact of A2T and D23N mutations on C99 homodimer conformations

Yan Lu, Freddie R Salsbury, Philippe Derreumaux

► **To cite this version:**

Yan Lu, Freddie R Salsbury, Philippe Derreumaux. Impact of A2T and D23N mutations on C99 homodimer conformations. *The Journal of Chemical Physics*, 2022, 157 (8), pp.085102. 10.1063/5.0101622 . hal-03775442

HAL Id: hal-03775442

<https://hal.sorbonne-universite.fr/hal-03775442v1>

Submitted on 12 Sep 2022

HAL is a multi-disciplinary open access archive for the deposit and dissemination of scientific research documents, whether they are published or not. The documents may come from teaching and research institutions in France or abroad, or from public or private research centers.

L'archive ouverte pluridisciplinaire **HAL**, est destinée au dépôt et à la diffusion de documents scientifiques de niveau recherche, publiés ou non, émanant des établissements d'enseignement et de recherche français ou étrangers, des laboratoires publics ou privés.

Impact of A2T and D23N mutations on C99 homodimer conformations

Yan Lu,¹ Freddie R. Salsbury Jr.,² and Philippe Derreumaux³

¹*School of Physics, Xidian University, Xi'an, 710071, China*^{a)}

²*Department of Physics, Wake Forest University, Winston-Salem, NC 27106, USA*

³*CNRS, Université Paris Cité, UPR 9080, Laboratoire de Biochimie Théorique, 13 rue Pierre et Marie Curie, Institut de Biologie Physico-Chimique, Fondation Edmond de Rothschild, 75005, Paris, France*^{b)}

The proteolytic cleavage of C99 by γ -secretase is the last step in the production of amyloid- β ($A\beta$) peptides. Previous studies have shown that membrane lipid composition, cholesterol concentration, and mutation in the transmembrane helix modified the structures and fluctuations of C99. In this study, we performed atomistic molecular dynamics simulations of the homodimer of the 55-residue congener of the C-terminal domain of the amyloid protein precursor, C99(1-55), in a POPC-cholesterol lipid bilayer, and we compared the conformational ensemble of WT sequence to those of the A2T and D23N variants. These mutations are particularly interesting as the protective Alzheimer's disease (AD) A2T mutation is known to decrease $A\beta$ production, whereas the early onset AD D23N mutation does not affect $A\beta$ production. We found noticeable differences in the structural ensembles of the three sequences. In particular, A2T varies from both WT and D23N by having long-range effects on the population of the extracellular justamembrane helix, the interface between the G29xxx-G33xxx-G37 motifs and the fluctuations of the transmembrane helical topologies.

Keywords: APP, C99, A2T and D23N mutations, Alzheimer's disease, amyloid simulations

^{a)}Electronic mail: luyan@xidian.edu.cn

^{b)}Institut Universitaire de France (IUF), 75005, Paris, France; Electronic mail: philippe.derreumaux@ibpc.fr

I. INTRODUCTION

The misfolding and early aggregation steps of the $A\beta$ peptides play a central role in Alzheimer disease (AD) and cerebral amyloid angiopathy.^[1,2] The cleavage of APP by β -secretase produces C99, and its subsequent sequential cleavage by γ -secretase produces different $A\beta$ forms varying from 37 to 46 residues in length, including $A\beta_{40}$ the most abundant alloform, and $A\beta_{42}$ the most toxic species.^[3-5]

C99 consists of an extracellular region, including a N-terminal domain, an extracellular justamembrane (JM) helical domain (residues 15-21), a loop region (residues 22-28), a transmembrane (TM) domain spanning residues 29-53 which contains two dimerization-inducing G-x-x-x-G motifs, and an intracellular C-terminal domain.^[6] The sequential cleavage mode of C99 with alternative initiation and proteolysis sites depends on many factors, such as peptide sequences, membrane properties, and structures and stabilities of the TM domain, among others.^[6-10]

C99 dimerization was proposed to lead to a change in the $A\beta$ ratio.^[11-13] C99 dimer structure diversity, ranging from right-handed coiled coil to left-handed coiled coil, was suggested to play an important role in APP processing and the distribution of $A\beta$ alloforms based on NMR and simulations in different membrane environments.^[14-18] A recent study demonstrated that the C99 dimer containing the G33-x-x-x-G37 motif in the interface promoted the $A\beta_{42}$ processing line and the dimer exhibiting the G25-x-x-x-G29 motif in the interface favored processing to $A\beta_{43/40}$.^[19]

Membrane composition is also important in APP processing and $A\beta$ production, and impacts the conformational ensemble of C99.^[6,9] Membrane-rich in omega-3 polyunsaturated fatty acids (PUFA) reduces $A\beta$ production, whereas membrane-rich in omega-6 increases the secretion of $A\beta$.^[20] All-atom molecular dynamics (MD) simulations revealed that both PUFA change the orientations and conformations of C99(15-55) homodimer.^[21] Membrane-rich in cholesterol causes an increase in $A\beta$ secretion,^[22,23] and the impact of cholesterol concentration on C99(16-55) monomer and homodimer was investigated by atomistic and coarse-grained MD simulations of C99(16-55).^[24,25] It was found that C99-cholesterol interfaces depend on C99 tilt angle and orientation of the JM domain, and there is no specific C99-cholesterol dimerization interface.^[25] Overall, many experimental and computational studies are conducted to understand the heterogeneous conformational ensemble of C99 fragments and its

full-length.²⁶

The link between γ -secretase cleavage, flexibility of the TM helix, C99 dimerization and mutations is being studied. Mutations of G29 and G33 reduce A β 42 production¹⁸ and are suggested to reduce C99 dimerization.²⁷ K28A mutation shifts A β alloform production from A β 40 to A β 33.²⁸ On the basis of a combined experimental (CD and NMR) and all-atom MD simulation in a POPC bilayer, Steiner et al. found that both de novo G38L and G38P mutations strongly reduced cleavage assay. Yet G38L led to a globally more stable TM helix, and G38P reduced its overall helicity.²⁹ Interestingly this MD simulation and previously described simulations revealed that the residues T43-I45 upstream the initiation sites provide additional hinge flexibility.³⁰

Many familial AD (FAD) mutations leading to early onset AD are located in the N-terminus (A2V, H6R, D7H, D7N), the C-terminal end of the central hydrophobic core (A21G) and the loop region (E22K, E22Q, E22G, D23N) of A β peptide. From biophysical and computational studies, it was observed that these mutations promote A β fibrillogenesis by altering the conformational ensemble of monomer and dimer in the bulk solution, the oligomer size distribution during the lag phase and the elongation and secondary nucleation rates.³¹⁻³⁶

Among these FAD mutations, D23N mutation is linked with severe cerebral amyloid angiopathy in a lowa kindred,³⁷ but does not affect A β production.³⁸ Many studies reported on its impact on fibril structures, the early aggregation steps in the bulk solution, the dissociation from a fibril, and the stability of preformed aggregates.³⁹⁻⁴⁷ Recently, its impact on the association of C99(16-55) monomer and cholesterol was investigated computationally.²⁵ In contrast to the early onset AD mutations, A2T mutation has a protective effect against AD,⁴⁸ decreases A β production,⁴⁸ and delays amyloid fibril formation.⁴⁹ A2T was studied to characterize the transition between disordered monomers and fibrils, and variations in oligomer size distribution, and aggregation kinetics,⁴⁹⁻⁵⁵ but no NMR experiments and MD simulations were conducted on A2T C99.

In this study, we performed atomistic MD simulations of the homodimer of the 55-residue congener of the C-terminal domain of APP, C99(1-55), in a POPC (1-palmitoyl-2-oleoyl-sn-glycero-3-phosphocholine)-cholesterol bilayer, and compared the conformational ensemble of WT sequence to those of the A2T and D23N variants. For each species, we carried out five simulations, each of 2 microseconds.

II. MATERIAL AND METHODS

The WT sequence of C99(1-55), which corresponds to $A\beta$ (1-55), is shown in FIG. 1. The N and C termini were capped by NH_3^+ and COO^- groups. The full structure of C99(1-55) was generated by MODELLER program⁵⁶ based on PDB 2LOH, C99(17-55). MODELLER implements an automated approach to comparative protein structure modeling by satisfaction of spatial restraints from the known related structures and their alignment with the target sequence. The form of these restraints are obtained from a statistical analysis of the relationships between many pairs of homologous structures.

The dimer was embedded into a membrane with 80% POPC and 20% cholesterol using CHARMM-GUI program⁵⁷ with a membrane thickness of 4.2 nm, and a 3.5 nm thickness of water molecules on each side of the membrane. We used the same construction and starting structure for the A2T and D23N variants. Overall the dimension (x, y and z) of the system is (7.6 nm, 7.6 nm, and 11.2 nm). The initial conformation of the system is shown in Fig. 1. POPC was selected because past simulations of C99 used this lipid,^{8,9} and the cholesterol ratio was selected because it is representative of its amount in cell membranes,⁵⁸ and was used in previous simulation of C99²⁵.

Molecular dynamics simulations were performed by using GROMACS 5.1.2.⁵⁹ Most past simulations on C99 employed CHARMM36 force field.^{9,25} In this work, the force field is Amber ff99SB*-ILDN⁶⁰ for the peptide, Slipids⁶¹⁻⁶³ for the membrane, and TIP3P for water,⁶⁴ as the combination of these three force fields was demonstrated to reproduce the experimental conformational ensemble of transmembrane proteins.⁶² The capability of the Amber ff99SB*-ILDN force field to reproduce the conformational ensemble of $A\beta$ in solution was also reported.⁶⁵ The temperature was kept at 310 K, by using V-rescale thermostat⁶⁶ and a coupling constant of 0.5 ps. Pressure was kept semi-isotropically at 1 atm by using Parrinello-Rahman barostat⁶⁷ with a coupling constant of 2 ps. All bonds were constrained using LINCS algorithm⁶⁸ with a 2 fs integration time step. A cutoff of 1.0 nm was used for Van der Waals interactions, and a cutoff of 1.0 nm for electrostatic interactions using the particle-mesh Ewald method.⁶⁹ We performed five runs for each system, each for 2000 ns, representing a total simulation time of 30 μs . The last 1800 ns of all simulations were used for analysis. Simulations were performed at neutral pH, representative of the plasma membrane environment and allowing comparison with previous simulations of C99.^{8,9} The

impact of acidic pH protonation states of E22 and D23, representative of the environment of endosomes, was reported in Refs.^{[25][70]}

The conformational ensemble of WT, A2T and D23N C99(1-55) homodimers was analyzed by various parameters. These include the secondary structure using the DSSP program,^[71] the distribution of the crossing angle between the two TM helices, as defined as the angle between the two vectors formed by the C α atoms joining residues 30 and 52, and the distribution of the crossing angle between the JM helix (residues 15-21) and the C-terminal TM helix spanning residues 29-36. A JM helix was considered formed if the rise per helical residue is 0.15 nm. The flexibility of the TM helix along the sequence was estimated by the C α root-mean-square fluctuations (RMSF) about the averaged MD structure.

The conformational ensemble was also characterized by 1D and 2D probability maps, the insertion depth of residues 1-28 into the bilayer, and several 2D free energy landscapes (FELs). The 2D free energy surfaces were constructed using the formula $-RT \times \log(H(x, y))$, where $H(x, y)$ is the histogram of the two selected parameters x and y .^[72] Finally, clustering of the full structures was performed using the Daura’s algorithm as implemented in GROMACS with a C α root-mean square deviation (RMSD) cutoff of 0.3 nm. Snapshots were created by using VMD package.^[73] The interactions of cholesterol with C99, proposed to be important as suggested by Sanders et al.,^[14] have been analyzed in Refs.^{[25][26]}

III. RESULTS AND DISCUSSION

Simulation convergence was checked using the first half of all trajectories (200-1100 ns) and the second half of all trajectories (1100-2000 ns). As reported in Supplementary Information, the secondary structure compositions of the extracellular (Table S1) and intracellular (Table S2) domains, and the probability distributions of the crossing angle of the TM helices (Fig. S1) are independent of the time interval. We also controlled that differences between WT and mutants are observed in each simulation, as reported by the probability distributions of the crossing angle between the JM and C-terminal TM helices (Fig. S2), and the probability distributions of the intermolecular C α K28K28 distance (Fig. S3). All together, these data provide the proof that the conformational ensembles of the three sequences are not due to insufficient sampling or convergence issues.

We first reported on the secondary structure content of the extracellular domain for the

three systems (Table I). All secondary structure components (coil, beta-sheet, beta-bridge, bend, turn, alpha-helix, Pi-helix and 3-10 helix) are very similar between the WT and D23N sequences. They display small differences in alpha-helix content (23.3% for WT vs 19.4% for D23N) and bend content (13.7% for WT vs 17.6% for D3N). Analysis of the secondary structure along the amino acid sequence in FIG. 2(a) shows an increase of alpha-helix (difference of 20 percents) in the region 18-23 and a decrease of alpha-helix (difference of 40 percents) in the region 24-27 upon D23N. Upon D23 mutation, there is an increase (difference of 10 percents) for the 3-10 helix at residues 3-10 (FIG. 2(b)), and the beta-sheet content slightly decreases (1.7% vs 4.0% for WT), mostly impacting residues 10 and 16-17 (FIG. 2(c)). The bend+turn content is higher for D23N (36.4%) than WT (30.2%), and impacts all residues 3-27 (FIG. 2(d)).

The secondary structure components change between the WT and A2T sequences (Table I). The (coil, alpha-helix and bend) contents amount to (43.9, 6.2 and 23.6%) in A2T vs (36.2, 23.3 and 13.7%) in WT. The reduction of alpha-helix impacts all residues, the exception being residue 28 (FIG. 2(a)). The A2T mutation augments and decreases the 3-10 helix content of residues 15-27 and 2-12, respectively (FIG. 2(b)). The bend+turn is much higher in A2T (39.2%) than in WT (30.2%), and impacts all residues 3-27. Overall, the JM helix content is slightly higher in WT than in D23N and is largely reduced in A2T species.

Table III gives the secondary structure content of the TM domain. In the three systems, the 3-10 helix content is very marginal, and the turn+bend content remains constant on the order of 4-6%. D23N slightly destabilizes the alpha-helix content (83%) and notably residues 29-30 (FIG. S4(a)) compared to WT and A2T sequences (86.4 and 85.1%). In all systems, the C-terminal residues 50-53 lose their helix content varying from 90% to 12%, and prefer bend+turn (FIG. S4(b)). The flexibility of the TM helices was evaluated by the crossing angle between the helices and the RMSF along the sequence. As seen in FIG. 3 the distributions of the crossing angle between the two TM helices in A2T and D23N mutants superpose very well and are shifted to slightly higher values than in WT (peak at 25° in A2T and D23N vs 21° in WT). It is noted that the distribution is more Gaussian-like than in the simulation of C99(29-42) homodimer in POPC.²¹ There are no significant differences between the three RMSFs, even if A2T displays more mobility than WT and then D23N (FIG. S5). The flexibility comes from the interactions between the two chains, and not from a single chain. The lowest RMSF surprisingly occurs at the G37G38 hinge residues, and residue

A42. Overall, the high helicity and the crossing angle distribution of the two TM helices are insensitive to A2T and D23N mutations. Our results are consistent with MD simulation of WT and D23N C99(16-55) monomers with different cholesterol concentrations.²⁵

Next we determined the FEL of the three systems projected onto d_{GG} and Φ_{4G} , as the GxxxG motif is known to promote helical dimerization.⁷⁴ d_{GG} is the distance between the two $C\alpha$ atoms of G33, and Φ_{4G} is the dihedral angle formed by G29-G37-G37-G29, as schematically shown in FIG. 4(a). FIG. 4(b)-(d) show the resulting FEL for WT, A2T and D23N. The WT FEL displays three free energy minima, denoted as w1, w2 and w3 with median values of Φ_{4G} and d_{GG} , and populations of $(-23.4^\circ, 1.62 \text{ nm}, 20.9\%)$, $(-17.9^\circ, 1.47 \text{ nm}, 13.7\%)$, and $(0.2^\circ, 1.31 \text{ nm}, 11.5\%)$ respectively. The A2T FEL displays one unique minimum, denoted as a1, with values of $(0.4^\circ, 1.41 \text{ nm}, 57.1\%)$, whereas the D23N FEL points to two minima, denoted as d1 and d2, with values of $(-14.1^\circ, 1.73 \text{ nm}, 15.8\%)$ and $(1.2^\circ, 1.42 \text{ nm}, 44.0\%)$.

Overall, the w1 and w2 minima are consistent with a NMR structure of WT C99(23-55) homodimer in a micelle (Φ_{4G} of -25° and d_{GG} of 1.4nm).¹⁵ In all minima, glycine repeats face the outside of the homodimer, d_{GG} varying between 1.4 and 1.6 nm, and correspond to the Gly-out state.⁹ Values of 1.5 nm were found in previous MD simulations of C99(29-42) and C99(15-55) homodimer in a pure POPC bilayer.^{21,75} There are notable differences in the three FELs. A2T C99(1-55) displays much less freedom around its unique minimum than its WT and D23N counterparts for both d_{GG} and Φ_{4G} parameters. All basins are rather narrow ($\Delta\Phi_{4G}$ on the order of $\pm 10^\circ$), the exception being state d2 in D23N with Φ_{4G} varying between -40 and $+23^\circ$. WT C99(1-55) has a very strong preference for right-handed coiled-coil geometries (negative values of Φ_{4G}), consistent with a NMR structure in a micelle.¹⁵ The positive Φ_{4G} values account for 18% of all states in WT. The A2T and D23N systems populate both right-handed and left-handed coiled-coils. A2T has the same probability for both coiled-coil states, while D23N displays a slight preference for right-handed coiled-coil geometries, the positive Φ_{4G} values accounting for 52% and 32% of all states for A2T and D23N, respectively.

We examined the impact of the two mutations on the hinge bending at G37G38, as this hinge has been conjectured to be important for $A\beta$ processing.^{17,76,77} The FEL was projected onto the tilt angle which is the angle between the vector L52A30 and z axis, and the kink angle at G37, which is the angle between the vectors L52G37 and G37A30, as schematically

shown in FIG. 5(a). The three FELs shown in FIG. 5(b)-(d) are nearly identical, displaying one global minimum and median values of the (tilt and kink) angles at (11.4° and 12.9° for WT), (12.1° and 14.2° for A2T) and (12.6° and 14.2° for D23N). D23N exhibits, however, a wider distribution than WT and A2T, and WT has the smallest distribution. We emphasize that the high similarity of the three FEL’s does not result from sampling, as MD simulations of 1 μ s on C99(15-55) homodimer show significant differences between the FEL(tilt angle, kink angle) in pure POPC, omega-3 and omega-6 membrane environments.²¹

To further explore TM dimerization, we calculated the 2D probability distance maps of the C α K28A-K28B distances (where A and B correspond to the two chains) and C α K54A-K54B distances. We used the terminology defined by Dominguez et al.¹⁷ for two topologies, namely parallel or ll (small values of the two distances < 0.8 nm), and λ (small KK28 distance < 0.8 nm and large KK54 distance > 1.1 nm). For large KK28 distance > 1.1 nm and small KK54 distance < 0.8 nm, the topology is V-like rather than Y-like, and for values > 1.1 nm of the two distances, the topology is bent-twisted (BT) rather than X-like. As shown in FIG. 6(a)-(c), WT simulation explores λ (population of 21%) and BT (19%) topologies, and then the V topology (11%). D23N simulation captures V and BT topologies (population of 26% and 24%) and then λ (14%). A2T simulation samples BT and V topologies with population of 29% and 23%, and λ with a population of 7.5%. In all systems, the population of the ll topology is rather small, amounting to (0.9%, 5.4% and 0.1%) for WT, A2T and D23N, respectively. Representative structures of the four topologies are shown in FIG. 6.

Overall, there are substantial differences between the 2D probability maps. The three sequences explore the λ , BT and V topologies with different populations. A2T is the single sequence to populate the ll topology. The V states in D23N and WT display much larger fluctuations of KK28 distances (variation between 1.5 and 2.2-2.6 nm) than in A2T (variation between 1.2 and 1.4 nm). The high probability of WT for the λ topology was reported in a previous simulation of C99(15-55) homodimer in pure POPC.¹⁷ Variation in topology description between the two simulations may result from differences in the amino acid length, membrane composition and force field.

Homodimer structures were characterized by the distributions of the crossing angle between the JM helix and the N-terminal of TM helix (FIG. 7). The distribution features two peaks in WT, whereas the distribution displays one dominant peak in A2T and D23N. The

mean and standard deviation is $44\pm 19^\circ$, $73\pm 14^\circ$ and $91\pm 18^\circ$ for WT, A2T and D23N respectively. WT and D23N display the smallest and largest average crossing angles, respectively.

Experimental and computational studies in different membrane compositions have reported on transient insertion of the JM helix into the membrane.^{61,70} FIG. 8(a) reports on the probability of each residue spanning the extracellular region to be inserted into the membrane, and FIG. 8(b) shows the average insertion depth of all residues 1-28. We observe that the N-terminal residues 1-11 of all species have almost a probability of 100% to lie above the membrane. The probability of JM helix to be inserted increases in the following order: D23N > A2T > WT. A probability of insertion > 12.5% involves the JM residues 15, 16, 17, 18, 20 and 21 in the D23 system, and residues 17, 18 and 20 in the A2T system. In the WT system, residues 15, 17, 18 and 21 also show insertion events, but with lower probabilities. Overall, the D23N and A2T mutations increase the crossing angle between the JM and TM helices, and the insertion of the JM helix into the membrane. Our predicted insertion profile of the JM helix for WT sequence is in agreement with EPR and NMR chemical shifts.⁶

Finally, we performed cluster analysis using the full sequence. The centers of the first five clusters of each sequence are shown in FIG. S6 and the cross RMSD deviations are shown in Table S3. Clusters 6-10 are not shown. The first ten clusters account for 36.4%, 43.9%, and 44.6% of all the conformations for WT, A2T and D23N, respectively. Of note, a few clusters display JM helices and transient beta-strands in the three sequences. Clusters 3 and 7 of WT with a total population of 5.9% show an extension of the TM helix on the N-terminal end spanning residues 16-51 in one chain and 19-52 in the second chain, allowing the formation of a G25xxxG29 interface. This event is however rare as it is observed in one single trajectory of WT. Transient beta-strands in the extracellular domain were reported on the basis of NMR and FTIR experiments on the WT and A21G C99(1-55),⁷⁸ and recent simulation of the full-length WT C99 monomer.²⁶ An extension of the TM helix from residues 30-53 to 26-55 was reported by increasing the z dimension of the lipid bilayer,²⁶ but an extension of 14 residues has never been reported. Overall, the long-range effects of A2T mutation on the conformational ensemble of C99 result from a different balance between the insertion probability into the membrane (and thus solvent accessibility) of the extracellular domain and the intermolecular forces between the two chains: the two TM helices and the two N-terminal regions, as shown in FIG. S7 which reports on the intermolecular side chain side chain contact probability maps between residues 1-23. The long-range effect of mutation at

position 2 was already reported in the simulations of A2V A β 28 monomer,⁷⁹ and A2T:WT A β 40 dimer⁵³ in the bulk solution.

IV. CONCLUSIONS

We have investigated the effects of A2T and D23N mutations on the conformations of C99(1-55) homodimer embedded in membrane by using all-atom MD simulations. Multiple parameters were analyzed in order to determine the link between A β production and conformational properties. We found that variation in A β production between the three sequences cannot be explained by the hinge bending at G37G38, the helical content of the TM helix, and the population of right-handed and left-handed coiled coil geometries. In contrast, we found that A2T varies from both WT and D23N sequences by having long-range effects on the population of the extracellular JM helix, the interface between the G29xxx-G33xxx-G37 motifs and the fluctuations of the TM helical topologies. Whether these conformational differences are sufficient to explain difference in A β production between A2T and (WT, D23N) remains to be determined, as other factors may alter the presentation of substrate to the proteolytic enzyme changing the initial ϵ -cleavage site.^{48,50} To further explore the link between A β production rate and conformational ensemble, it would be interesting to perform C99(1-55) homodimer simulations of the A21G and E22G mutations in in vivo mimicking-membrane environment.

V. SUPPLEMENTARY MATERIAL

See supplementary material for the secondary structure compositions of the extracellular (Table S1) and intracellular (Table S2) domains in different time intervals, the cross RMSD among the centers of the first five clusters (Table S3), the probability distributions of the crossing angle of the TM helices in different time intervals (Fig. S1), the probability distributions of the crossing angle between the JM and C-terminal TM helices for different simulations (Fig. S2), the probability distributions of the intermolecular C α K28K28 distance (Fig. S3) for different simulations, secondary structure content of the intracellular domain (Fig. S4), RMSF of the intracellular domain (Fig. S5), The centers of the first five clusters (FIG. S6), and the intermolecular side chain side chain contact probability maps

between residues 1-23 (Fig. S7).

VI. ACKNOWLEDGEMENTS

This research is supported by the National Natural Science Foundation of China under Grant No. 11804262, the Natural Science Basic Research Program of Shaanxi Province of China under Grant No. 2020JQ-287, and the Fundamental Research Funds for the Central Universities. Computations were performed on the Wake Forest University DEAC Cluster, a centrally managed resource with support provided in part by the University, and on the HPC system of Xidian University. PD thanks the support of the “Initiative d’Excellence” program from the French State, Grant “DYNAMO”, ANR-11-LABX-0011-01.

REFERENCES

- ¹S. M. Greenberg, B. J. Bacskai, M. Hernandez-Guillamon, J. Pruzin, R. Sperling, and S. J. van Veluw, “Cerebral amyloid angiopathy and Alzheimer disease - one peptide, two pathways.” [Nat Rev Neurol **16**, 30–42 \(2020\)](#).
- ²D. J. Selkoe and J. Hardy, “The amyloid hypothesis of Alzheimer’s disease at 25 years.” [EMBO Mol Med **8**, 595–608 \(2016\)](#).
- ³S. Funamoto, M. Morishima-Kawashima, Y. Tanimura, N. Hirotsu, T. C. Saido, and Y. Ihara, “Truncated Carboxyl-Terminal Fragments of β -Amyloid Precursor Protein Are Processed to Amyloid β -Proteins 40 and 42,” [Biochemistry **43**, 13532–13540 \(2004\)](#).
- ⁴P. H. Nguyen, A. Ramamoorthy, B. R. Sahoo, J. Zheng, P. Faller, J. E. Straub, L. Dominguez, J.-E. Shea, N. V. Dokholyan, A. D. Simone, B. Ma, R. Nussinov, S. Najafi, S. T. Ngo, A. Loquet, M. Chiricotto, P. Ganguly, J. McCarty, M. S. Li, C. Hall, Y. Wang, Y. Miller, S. Melchionna, B. Habenstein, S. Timr, J. Chen, B. Hnath, B. Strodel, R. Kaye, S. Lesné, G. Wei, F. Sterpone, A. J. Doig, and P. Derreumaux, “Amyloid Oligomers: A Joint Experimental/Computational Perspective on Alzheimer’s Disease, Parkinson’s Disease, Type II Diabetes, and Amyotrophic Lateral Sclerosis.” [Chem Rev **121**, 2545–2647 \(2021\)](#).
- ⁵Y. Qi-Takahara, M. Morishima-Kawashima, Y. Tanimura, G. Dolios, N. Hirotsu, Y. Horikoshi, F. Kametani, M. Maeda, T. C. Saido, R. Wang, and Y. Ihara, “Longer

- forms of amyloid beta protein: implications for the mechanism of intramembrane cleavage by gamma-secretase.” [J Neurosci **25**, 436–445 \(2005\)](#).
- ⁶P. J. Barrett, Y. Song, W. D. Van Horn, E. J. Hustedt, J. M. Schafer, A. Hadziselimovic, A. J. Beel, and C. R. Sanders, “The Amyloid Precursor Protein Has a Flexible Transmembrane Domain and Binds Cholesterol.” [Science **336**, 1168–1171 \(2012\)](#).
- ⁷T. Sato, T.-c. Tang, G. Reubins, J. Z. Fei, T. Fujimoto, P. Kienlen-Campard, S. N. Constantinescu, J.-N. Octave, S. Aimoto, and S. O. Smith, “A helix-to-coil transition at the ϵ -cut site in the transmembrane dimer of the amyloid precursor protein is required for proteolysis,” [Proceedings of the National Academy of Sciences **106**, 1421–1426 \(2009\)](#).
- ⁸L. Dominguez, S. C. Meredith, J. E. Straub, and D. Thirumalai, “Transmembrane Fragment Structures of Amyloid Precursor Protein Depend on Membrane Surface Curvature,” [Journal of the American Chemical Society **136**, 854–857 \(2014\)](#).
- ⁹L. Dominguez, L. Foster, J. E. Straub, and D. Thirumalai, “Impact of Membrane Lipid Composition on the Structure and Stability of the Transmembrane Domain of Amyloid Precursor Protein,” [Proceedings of the National Academy of Sciences **113**, E5281–E5287 \(2016\)](#).
- ¹⁰P. Kienlen-Campard, B. Tasiaux, J. Van Hees, M. Li, S. Huysseune, T. Sato, J. Z. Fei, S. Aimoto, P. J. Courtoy, S. O. Smith, S. N. Constantinescu, and J. N. Octave, “Amyloidogenic Processing but Not Amyloid Precursor Protein (APP) Intracellular C-Terminal Domain Production Requires a Precisely Oriented APP Dimer Assembled by Transmembrane GXXXG Motifs,” [Journal of Biological Chemistry **283**, 7733–7744 \(2008\)](#).
- ¹¹L.-M. Munter, P. Voigt, A. Harmeier, D. Kaden, K. E. Gottschalk, C. Weise, R. Pipkorn, M. Schaefer, D. Langosch, and G. Multhaup, “GxxxG motifs within the amyloid precursor protein transmembrane sequence are critical for the etiology of A β 42,” [The EMBO Journal **26**, 1702–1712 \(2007\)](#).
- ¹²P. M. Gorman, S. Kim, M. Guo, R. A. Melnyk, J. McLaurin, P. E. Fraser, J. U. Bowie, and A. Chakrabarty, “Dimerization of the transmembrane domain of amyloid precursor proteins and familial Alzheimer’s disease mutants,” [BMC Neuroscience **9**, 1–11 \(2008\)](#).
- ¹³N. B. Khalifa, J. V. Hees, B. Tasiaux, S. Huysseune, S. O. Smith, S. N. Constantinescu, J.-N. Octave, and P. Kienlen-Campard, “What is the role of amyloid precursor protein dimerization?” [Cell Adhesion & Migration **4**, 268–272 \(2010\)](#).

- ¹⁴A. J. Beel, C. K. Mobley, H. J. Kim, F. Tian, A. Hadziselimovic, B. Jap, J. H. Prestegard, and C. R. Sanders, “Structural Studies of the Transmembrane C-Terminal Domain of the Amyloid Precursor Protein (APP): Does APP Function as a Cholesterol Sensor?” [Biochemistry](#) **47**, 9428–9446 (2008).
- ¹⁵W. Chen, E. Gamache, D. J. Rosenman, J. Xie, M. M. Lopez, Y. M. Li, and C. Wang, “Familial Alzheimer’s mutations within APPTM increase A β 42 production by enhancing accessibility of ϵ -cleavage site,” [Nature Communications](#) **5**, 3037 (2014).
- ¹⁶K. D. Nadezhdin, O. V. Bocharova, E. V. Bocharov, and A. S. Arseniev, “Dimeric structure of transmembrane domain of amyloid precursor protein in micellar environment,” [FEBS Letters](#) **586**, 1687–1692 (2012).
- ¹⁷L. Dominguez, L. Foster, S. C. Meredith, J. E. Straub, and D. Thirumalai, “Structural Heterogeneity in Transmembrane Amyloid Precursor Protein Homodimer Is a Consequence of Environmental Selection,” [Journal of the American Chemical Society](#) **136**, 9619–9626 (2014).
- ¹⁸C.-D. Li, M. Junaid, H. Chen, A. Ali, and D.-Q. Wei, “Helix-Switch Enables C99 Dimer Transition Between the Multiple Conformations.” [J Chem Inf Model](#) **59**, 339–350 (2019).
- ¹⁹F. Perrin, N. Papadopoulos, N. Suelves, R. Opsomer, D. M. Vadukul, C. Vrancx, S. O. Smith, D. Vertommen, P. Kienlen-Campard, and S. N. Constantinescu, “Dimeric Transmembrane Orientations of APP/C99 Regulate γ -Secretase Processing Line Impacting Signaling and Oligomerization.” [iScience](#) **23**, 101887 (2020).
- ²⁰Z. Amtul, M. Uhrig, R. F. Rozmahel, and K. Beyreuther, “Structural Insight Into the Differential Effects of Omega-3 and Omega-6 Fatty Acids on the Production of Abeta Peptides and Amyloid Plaques.” [J. Biol. Chem.](#) **286**, 6100–6107 (2011).
- ²¹Y. Lu, X.-F. Shi, P. H. Nguyen, F. Sterpone, F. R. Salsbury, and P. Derreumaux, “Amyloid- β (29–42) Dimeric Conformations in Membranes Rich in Omega-3 and Omega-6 Polyunsaturated Fatty Acids,” [The Journal of Physical Chemistry B](#) **123**, 2687–2696 (2019).
- ²²L. M. Refolo, M. A. Pappolla, B. Malester, J. LaFrancois, T. Bryant-Thomas, R. Wang, G. Tint, K. Sambamurti, and K. Duff, “Hypercholesterolemia Accelerates the Alzheimer’s Amyloid Pathology in a Transgenic Mouse Model,” [Neurobiology of Disease](#) **7**, 321–331 (2000).

- ²³L. Puglielli, R. E. Tanzi, and D. M. Kovacs, “Alzheimer’s disease: the cholesterol connection,” [Nature neuroscience](#) **6**, 345–351 (2003).
- ²⁴A. D. Stange, J. P.-C. Hsu, L. K. Ravnkilde, N. Berglund, and B. Schiøtt, “Effect of cholesterol on the dimerization of C99-A molecular modeling perspective.” [Biointerphases](#) **16**, 031002 (2021).
- ²⁵G. A. Pantelopulos, A. Panahi, and J. E. Straub, “Impact of Cholesterol Concentration and Lipid Phase on Structure and Fluctuation of Amyloid Precursor Protein.” [J Phys Chem B](#) **124**, 10173–10185 (2020).
- ²⁶G. A. Pantelopulos, J. E. Straub, D. Thirumalai, and Y. Sugita, “Structure of APP-C991–99 and implications for role of extra-membrane domains in function and oligomerization,” [Biochimica et Biophysica Acta \(BBA\) - Biomembranes](#) **1860**, 1698–1708 (2018).
- ²⁷S. M. Anderson, B. K. Mueller, E. J. Lange, and A. Senes, “Combination of C α -H Hydrogen Bonds and van der Waals Packing Modulates the Stability of GxxxG-Mediated Dimers in Membranes.” [J Am Chem Soc](#) **139**, 15774–15783 (2017).
- ²⁸T. L. Kukar, T. B. Ladd, P. Robertson, S. A. Pintchovski, B. Moore, M. A. Bann, Z. Ren, K. Jansen-West, K. Malphrus, S. Eggert, H. Maruyama, B. A. Cottrell, P. Das, G. S. Basi, E. H. Koo, and T. E. Golde, “Lysine 624 of the Amyloid Precursor Protein (APP) Is a Critical Determinant of Amyloid β Peptide Length,” [Journal of Biological Chemistry](#) **286**, 39804–39812 (2011).
- ²⁹A. Götz, N. Mylonas, P. Högel, M. Silber, H. Heinel, S. Menig, A. Vogel, H. Feyrer, D. Huster, B. Luy, D. Langosch, C. Scharnagl, C. Muhle-Goll, F. Kamp, and H. Steiner, “Modulating Hinge Flexibility in the APP Transmembrane Domain Alters γ -Secretase Cleavage,” [Biophysical Journal](#) **116**, 2103–2120 (2019).
- ³⁰A. Götz, P. Högel, M. Silber, I. Chaitoglou, B. Luy, C. Muhle-Goll, C. Scharnagl, and D. Langosch, “Increased H-Bond Stability Relates to Altered ϵ -Cleavage Efficiency and A β Levels in the I45T Familial Alzheimer’s Disease Mutant of APP,” [Scientific Reports](#) **9**, 1–12 (2019).
- ³¹J. Nasica-Labouze, P. H. Nguyen, F. Sterpone, O. Berthoumieu, N.-V. Buchete, S. Coté, A. De Simone, A. J. Doig, P. Faller, A. Garcia, A. Laio, M. S. Li, S. Melchionna, N. Mousseau, Y. Mu, A. Paravastu, S. Pasquali, D. J. Rosenman, B. Strodel, B. Tarus, J. H. Viles, T. Zhang, C. Wang, and P. Derreumaux, “Amyloid β Protein and Alzheimer’s Disease: When Computer Simulations Complement Experimental Studies,” [Chemical Re-](#)

-
- views **115**, 3518–3563 (2015).
- ³²P. H. Nguyen, F. Sterpone, J. M. Campanera, J. Nasica-Labouze, and P. Derreumaux, “Impact of the A2V Mutation on the Heterozygous and Homozygous A β 1–40 Dimer Structures From Atomistic Simulations,” *ACS Chemical Neuroscience* **7**, 823–832 (2016).
- ³³L. Aggarwal and P. Biswas, “Hydration Thermodynamics of the N-Terminal FAD Mutants of Amyloid- β ,” *Journal of Chemical Information and Modeling* **61**, 298–310 (2021).
- ³⁴B. Sharma, S. V. Ranganathan, and G. Belfort, “Weaker N-Terminal Interactions for the Protective over the Causative A β Peptide Dimer Mutants,” *ACS Chemical Neuroscience* **9**, 1247–1253 (2018).
- ³⁵M. Messa, L. Colombo, E. del Favero, L. Cantù, T. Stoilova, A. Cagnotto, A. Rossi, M. Morbin, G. Di Fede, F. Tagliavini, and M. Salmona, “The Peculiar Role of the A2V Mutation in Amyloid- β (A β) 1–42 Molecular Assembly*,” *Journal of Biological Chemistry* **289**, 24143–24152 (2014).
- ³⁶M. H. Viet, P. H. Nguyen, P. Derreumaux, and M. S. Li, “Effect of the English Familial Disease Mutation (H6R) on the Monomers and Dimers of A β 40 and A β 42,” *ACS Chemical Neuroscience* **5**, 646–657 (2014).
- ³⁷T. J. Grabowski, H. S. Cho, J. P. Vonsattel, G. W. Rebeck, and S. M. Greenberg, “Novel amyloid precursor protein mutation in an Iowa family with dementia and severe cerebral amyloid angiopathy.” *Ann Neurol* **49**, 697–705 (2001).
- ³⁸W. E. V. Nostrand, J. P. Melchor, H. S. Cho, S. M. Greenberg, and G. W. Rebeck, “Pathogenic effects of D23N Iowa mutant amyloid beta -protein.” *J Biol Chem* **276**, 32860–6 (2001).
- ³⁹X. Yang, G. Meisl, B. Frohm, E. Thulin, T. P. Knowles, and S. Linse, “On the role of sidechain size and charge in the aggregation of A β 42 with familial mutations,” *Proceedings of the National Academy of Sciences of the United States of America* **115**, E5849–E5858 (2018).
- ⁴⁰R. Tycko, K. L. Sciarretta, J. P. Orgel, and S. C. Meredith, “Evidence for novel β -sheet structures in Iowa mutant β -amyloid fibrils,” *Biochemistry* **48**, 6072–6084 (2009).
- ⁴¹Z. Fu, W. E. Van Nostrand, and S. O. Smith, “Anti-parallel β -hairpin structure in soluble a β oligomers of a β 40-dutch and A β 40-iowa,” *International Journal of Molecular Sciences* **22**, 1225 (2021).

- ⁴²A. Okamoto, A. Yano, K. Nomura, S. Higai, and N. Kurita, “Effect of D23N mutation on the dimer conformation of amyloid β -proteins: Ab initio molecular simulations in water,” [Journal of Molecular Graphics and Modelling](#) **50**, 113–124 (2014).
- ⁴³E. J. Alred, E. G. Scheele, W. M. Berhanu, and U. H. Hansmann, “Stability of Iowa mutant and wild type A β -peptide aggregates,” [Journal of Chemical Physics](#) **141**, 1–10 (2014).
- ⁴⁴S. Côté, R. Laghaei, P. Derreumaux, and N. Mousseau, “Distinct dimerization for various alloforms of the amyloid-beta protein: A β (1-40), A β (1-42), and A β (1-40)(D23N).” [J Phys Chem B](#) **116**, 4043–55 (2012).
- ⁴⁵R. A. Rodriguez, L. Y. Chen, G. Plascencia-Villa, and G. Perry, “Thermodynamics of Amyloid- β Fibril Elongation: Atomistic Details of the Transition State,” [ACS Chemical Neuroscience](#) **9**, 783–789 (2018).
- ⁴⁶P. H. Nguyen and P. Derreumaux, “Structures of the intrinsically disordered A β , tau and α -synuclein proteins in aqueous solution from computer simulations,” [Biophysical Chemistry](#) **264**, 106421 (2020).
- ⁴⁷S. T. Ngo, P. H. Nguyen, and P. Derreumaux, “Impact of A2T and D23N Mutations on Tetrameric A β 42 Barrel within a Dipalmitoylphosphatidylcholine Lipid Bilayer Membrane by Replica Exchange Molecular Dynamics,” [Journal of Physical Chemistry B](#) **124**, 1175–1182 (2020).
- ⁴⁸T. Jonsson, J. K. Atwal, S. Steinberg, J. Snaedal, P. V. Jonsson, S. Bjornsson, H. Stefansson, P. Sulem, D. Gudbjartsson, J. Maloney, K. Hoyte, A. Gustafson, Y. Liu, Y. Lu, T. Bhangale, R. R. Graham, J. Huttenlocher, G. Bjornsdottir, O. a. Andreassen, E. G. Jönsson, A. Palotie, T. W. Behrens, O. T. Magnusson, A. Kong, U. Thorsteinsdottir, R. J. Watts, and K. Stefansson, “A Mutation in APP Protects Against Alzheimer qs Disease and Age-Related Cognitive Decline,” [Nature](#) **488**, 96–99 (2012).
- ⁴⁹I. Benilova, R. Gallardo, A. A. Ungureanu, V. C. Cano, A. Snellinx, M. Ramakers, C. Bartic, F. Rousseau, J. Schymkowitz, and B. De Strooper, “The Alzheimer disease protective mutation A2T modulates kinetic and thermodynamic properties of amyloid- β (A β) aggregation,” [Journal of Biological Chemistry](#) **289**, 30977–30989 (2014).
- ⁵⁰L. Colombo, A. Gamba, L. Cantù, M. Salmona, F. Tagliavini, V. Rondelli, E. Del Favero, and P. Brocca, “Pathogenic A β A2V versus protective A β A2T mutation: Early stage aggregation and membrane interaction,” [Biophysical Chemistry](#) **229**, 11–18 (2017).

- ⁵¹B. Murray, M. Sorci, J. Rosenthal, J. Lippens, D. Isaacson, P. Das, D. Fabris, S. Li, and G. Belfort, “A2T and A2V A β peptides exhibit different aggregation kinetics, primary nucleation, morphology, structure, and LTP inhibition,” [Proteins: Structure, Function and Bioinformatics](#) **84**, 488–500 (2016).
- ⁵²L. Aggarwal and P. Biswas, “Effect of Alzheimer’s Disease Causative and Protective Mutations on the Hydration Environment of Amyloid- β ,” [Journal of Physical Chemistry B](#) **124**, 2311–2322 (2020).
- ⁵³P. H. Nguyen, F. Sterpone, R. Pouplana, P. Derreumaux, and J. M. Campanera, “Dimerization Mechanism of Alzheimer A β 40 Peptides: The High Content of Intra-peptide-Stabilized Conformations in A2V and A2T Heterozygous Dimers Retards Amyloid Fibril Formation,” [The Journal of Physical Chemistry B](#) **120**, 12111–12126 (2016).
- ⁵⁴P. Das, A. R. Chacko, and G. Belfort, “Alzheimer’s Protective Cross-Interaction between Wild-Type and A2T Variants Alters A β 42 Dimer Structure,” [ACS Chemical Neuroscience](#) **8**, 606–618 (2017).
- ⁵⁵X. Zheng, D. Liu, R. Roychaudhuri, D. B. Teplow, and M. T. Bowers, “Amyloid β - Protein Assembly: Differential Effects of the Protective A2T Mutation and Recessive A2V Familial Alzheimer’s Disease Mutation,” [ACS Chemical Neuroscience](#) **6**, 1732–1740 (2015).
- ⁵⁶A. Sali and T. L. Blundell, “Comparative protein modelling by satisfaction of spatial restraints.” [J. Mol. Biol.](#) **234**, 779–815 (1993).
- ⁵⁷S. Jo, J. B. Lim, J. B. Klauda, and W. Im, “CHARMM-GUI Membrane Builder for Mixed Bilayers and Its Application to Yeast Membranes,” [Biophysical Journal](#) **97**, 50–58 (2009).
- ⁵⁸J. Egawa, M. L. Pearn, B. P. Lemkuil, P. M. Patel, and B. P. Head, “Membrane lipid rafts and neurobiology: age-related changes in membrane lipids and loss of neuronal function,” [The Journal of Physiology](#) **594**, 4565–4579 (2016).
- ⁵⁹H. Berendsen, D. van der Spoel, and R. van Drunen, “GROMACS: A Message-Passing Parallel Molecular Dynamics Implementation,” [Computer Physics Communications](#) **91**, 43–56 (1995).
- ⁶⁰K. Lindorff-Larsen, S. Piana, K. Palmo, P. Maragakis, J. L. Klepeis, R. O. Dror, and D. E. Shaw, “Improved Side-Chain Torsion Potentials for the Amber ff99SB Protein Force Field,” [Proteins: Structure, Function and Bioinformatics](#) **78**, 1950–1958 (2010).

- ⁶¹J. P. M. Jämbeck and A. P. Lyubartsev, “Derivation and Systematic Validation of a Refined All-Atom Force Field for Phosphatidylcholine Lipids,” [Journal of Physical Chemistry B](#) **116**, 3164–3179 (2012).
- ⁶²J. P. M. Jämbeck and A. P. Lyubartsev, “An Extension and Further Validation of an All-Atomistic Force Field for Biological Membranes,” [Journal of Chemical Theory and Computation](#) **8**, 2938–2948 (2012).
- ⁶³J. P. M. Jämbeck and A. P. Lyubartsev, “Another Piece of the Membrane Puzzle: Extending Slipids Further,” [Journal of Chemical Theory and Computation](#) **9**, 774–784 (2013).
- ⁶⁴W. L. Jorgensen, J. Chandrasekhar, J. D. Madura, R. W. Impey, and M. L. Klein, “Comparison of Simple Potential Functions for Simulating Liquid Water,” [The Journal of Chemical Physics](#) **79**, 926–935 (1983).
- ⁶⁵M. Carballo-Pacheco and B. Strodel, “Comparison of force fields for Alzheimer’s A β 42: A case study for intrinsically disordered proteins.” [Protein Sci](#) **26**, 174–185 (2017).
- ⁶⁶H. J. C. Berendsen, J. P. M. Postma, W. F. van Gunsteren, A. DiNola, and J. R. Haak, “Molecular Dynamics With Coupling to an External Bath,” [The Journal of Chemical Physics](#) **81**, 3684–3690 (1984).
- ⁶⁷M. Parrinello and A. Rahman, “Polymorphic Transitions in Single Crystals: A New Molecular Dynamics Method,” [Journal of Applied Physics](#) **52**, 7182–7190 (1981).
- ⁶⁸B. Hess, H. Bekker, H. J. C. Berendsen, and J. G. E. M. Fraaije, “LINCS: A Linear Constraint Solver for Molecular Simulations,” [Journal of Computational Chemistry](#) **18**, 1463–1472 (1997).
- ⁶⁹U. Essmann, L. Perera, M. L. Berkowitz, T. Darden, H. Lee, and L. G. Pedersen, “A Smooth Particle Mesh Ewald Method,” [The Journal of Chemical Physics](#) **103**, 8577–8593 (1995).
- ⁷⁰A. Panahi, A. Bandara, G. A. Pantelopulos, L. Dominguez, and J. E. Straub, “Specific Binding of Cholesterol to C99 Domain of Amyloid Precursor Protein Depends Critically on Charge State of Protein,” [The Journal of Physical Chemistry Letters](#) **7**, 3535–3541 (2016).
- ⁷¹W. Kabsch and C. Sander, “Dictionary of Protein Secondary Structures,” [Biopolymers](#) **22**, 2577–2637 (1983).
- ⁷²Y. Lu, P. Derreumaux, Z. Guo, N. Mousseau, and G. Wei, “Thermodynamics and dynamics of amyloid peptide oligomerization are sequence dependent,” [Proteins: Structure, Function, and Bioinformatics](#) **75**, 954–963 (2009).

- ⁷³W. Humphrey, A. Dalke, and K. Schulten, “VMD: Visual Molecular Dynamics,” [Journal of Molecular Graphics](#) **14**, 33–38 (1996).
- ⁷⁴M. Audagnotto, T. Lemmin, A. Barducci, and M. D. Peraro, “Effect of the Synaptic Plasma Membrane on the Stability of the Amyloid Precursor Protein Homodimer,” [The Journal of Physical Chemistry Letters](#) **7**, 3572–3578 (2016).
- ⁷⁵Y. Lu, X.-F. Shi, F. R. Salsbury, and P. Derreumaux, “Influence of electric field on the amyloid- β (29-42) peptides embedded in a membrane bilayer,” [The Journal of Chemical Physics](#) **148**, 045105 (2018).
- ⁷⁶N. Miyashita, J. E. Straub, and D. Thirumalai, “Structures of Beta-Amyloid Peptide 1-40, 1-42, and 1-55-The 672-726 Fragment of APP-in a Membrane Environment With Implications for Interactions With Gamma-Secretase.” [J. Am. Chem. Soc.](#) **131**, 17843–17852 (2009).
- ⁷⁷O. Pester, P. J. Barrett, D. Hornburg, P. Hornburg, R. Pröbstle, S. Widmaier, C. Kutzner, M. Dürrbaum, A. Kapurniotu, C. R. Sanders, C. Scharnagl, and D. Langosch, “The Backbone Dynamics of the Amyloid Precursor Protein Transmembrane Helix Provides a Rationale for the Sequential Cleavage Mechanism of γ -Secretase.” [J. Am. Chem. Soc.](#) **135**, 1317–1329 (2013).
- ⁷⁸T.-C. Tang, Y. Hu, P. Kienlen-Campard, L. El Haylani, M. Decock, J. Van Hees, Z. Fu, J.-N. Octave, S. N. Constantinescu, and S. O. Smith, “Conformational Changes Induced by the A21G Flemish Mutation in the Amyloid Precursor Protein Lead to Increased A β Production,” [Structure](#) **22**, 387–396 (2014).
- ⁷⁹P. H. Nguyen, B. Tarus, and P. Derreumaux, “Familial Alzheimer A2V Mutation Reduces the Intrinsic Disorder and Completely Changes the Free Energy Landscape of the A β 1–28 Monomer,” [The Journal of Physical Chemistry B](#) **118**, 501–510 (2014).
- ⁸⁰S.-Y. Chen and M. Zacharias, “An internal docking site stabilizes substrate binding to γ -secretase: Analysis by molecular dynamics simulations.” [Biophys J](#) **121**, 2330–2344 (2022).

%	Coil	β -Sheet	β -Bridge	Bend	Turn	α -Helix	π -helix	3_{10} -helix
WT	36.2	4.0	0.9	13.7	16.6	23.3	0.0	5.2
A2T	43.9	1.7	2.9	23.6	15.7	6.2	0.0	5.8
D23N	35.3	1.7	0.9	17.6	18.8	19.4	0.3	5.9

TABLE I. Secondary structure composition of the extracellular domain (residues 1-28).

%	Coil	β -Sheet	β -Bridge	Bend	Turn	α -Helix	π -helix	3_{10} -helix
WT	9.5	0.0	0.0	1.7	2.3	86.4	0.0	0.1
A2T	9.9	0.0	0.0	1.9	2.8	85.1	0.0	0.2
D23N	10.7	0.0	0.1	2.2	3.7	83.0	0.0	0.2

TABLE II. Secondary structure composition of the transmembrane domain (residues 29-52) and residues K53-K55.

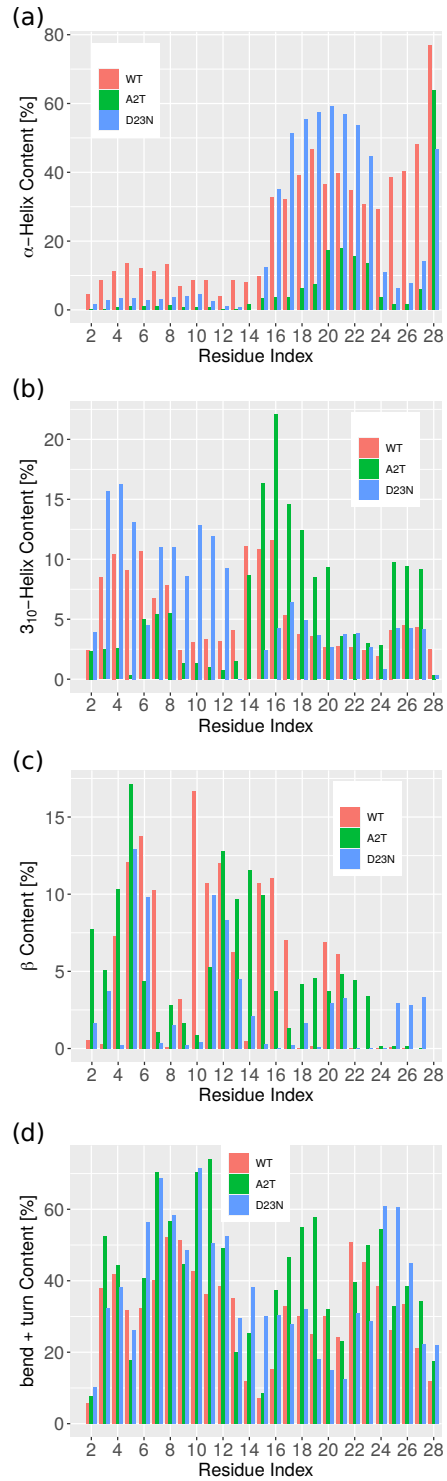


FIG. 2. Secondary structure content of the extracellular domain (residues 1-28). (a) α -helix, (b) 3_{10} -helix, (c) β (sheet + bridge) and (d) turn+bend.

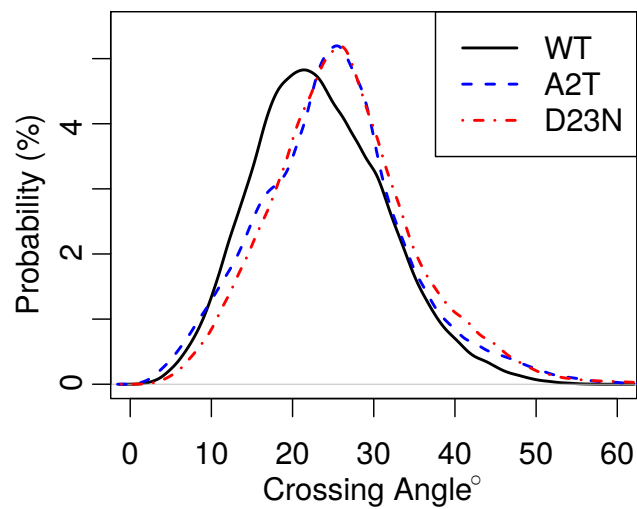


FIG. 3. Probability distributions of the crossing angle in degrees between the two TM helices.

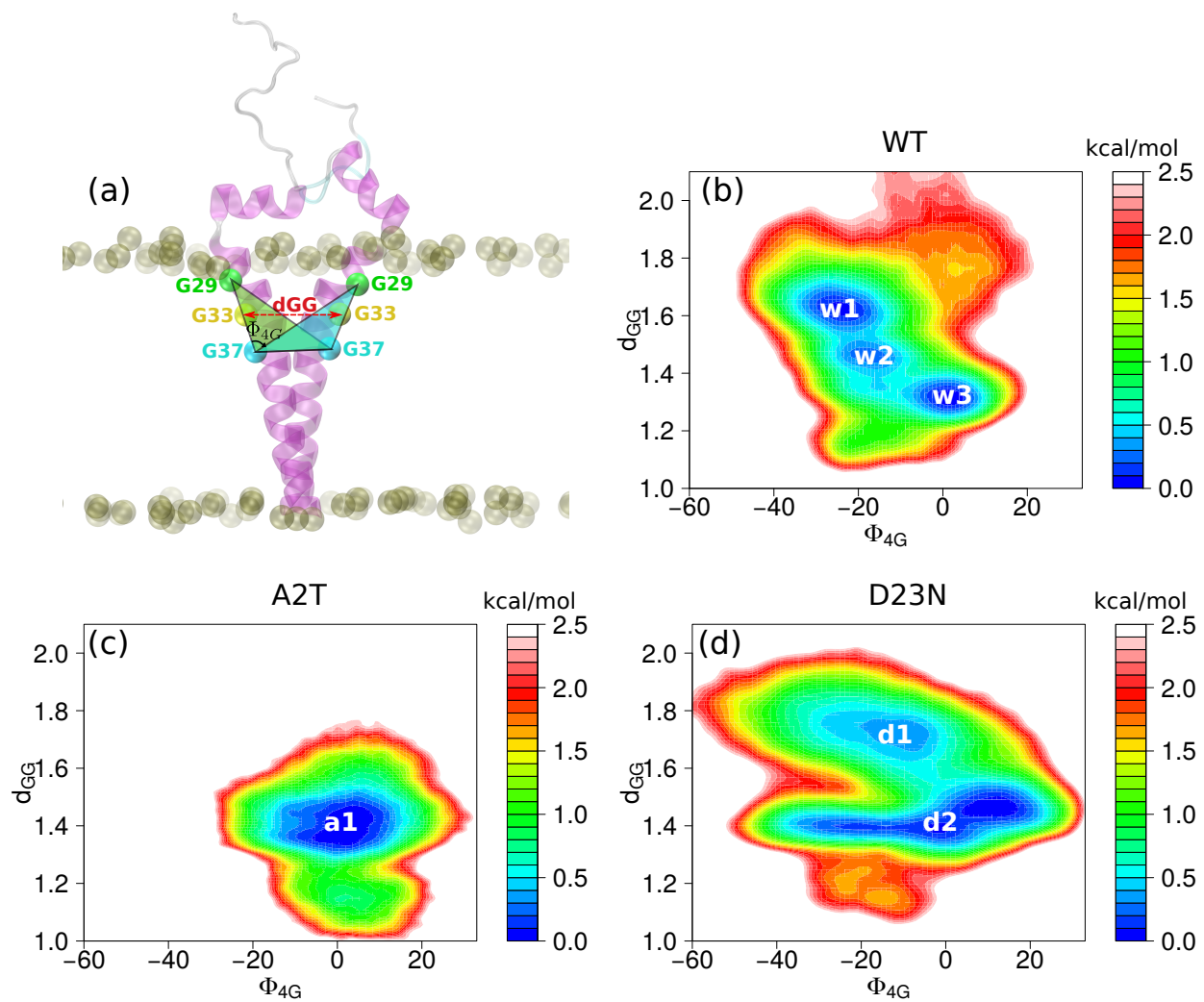


FIG. 4. Free energy landscape (FEL) projected onto d_{GG} and Φ_{4G} for the three sequences. (a) Definition of d_{GG} and Φ_{4G} . WT, A2T and D23N in (b), (c) and (d).

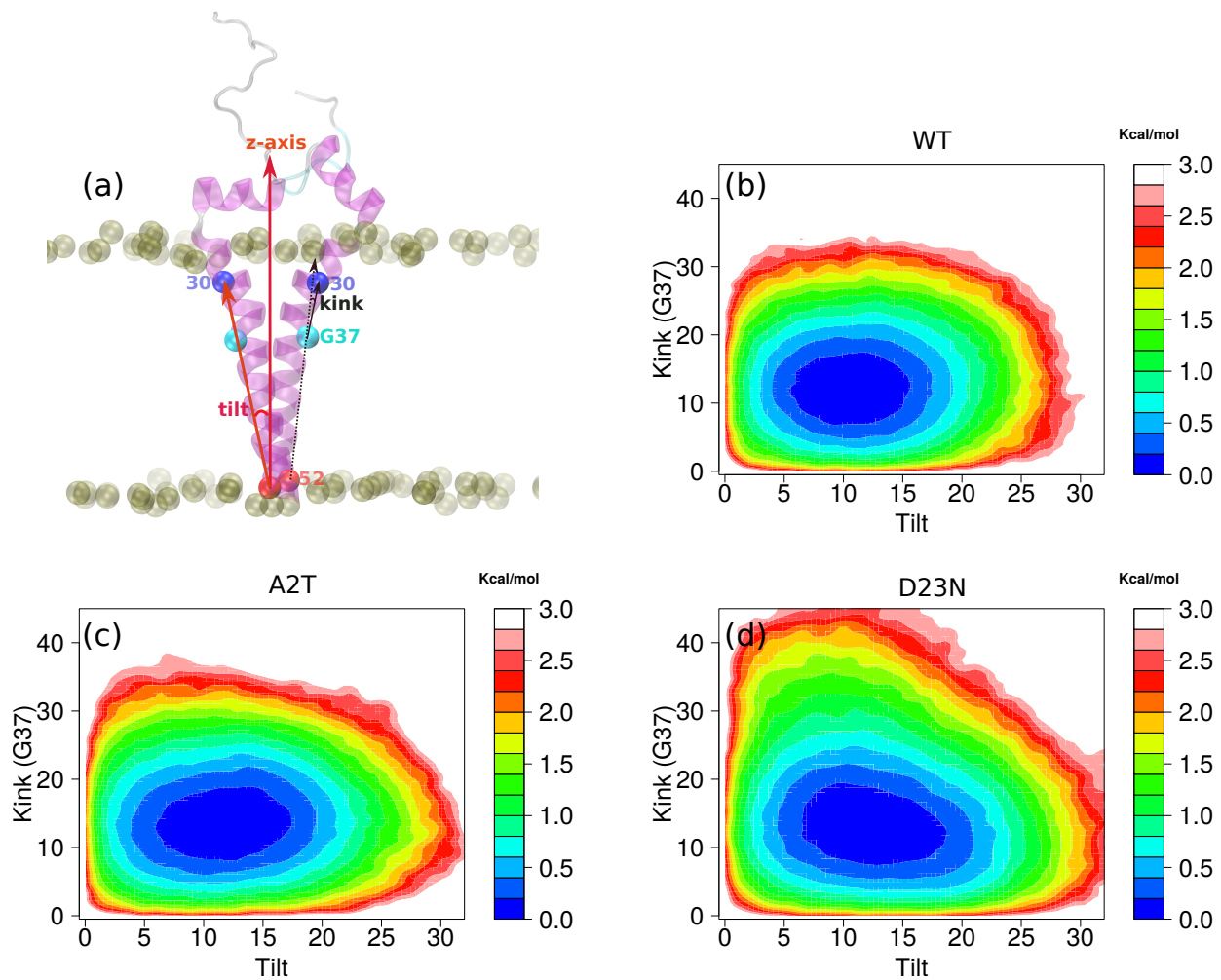


FIG. 5. Free energy landscape projected onto the tilt and kink angles for the three sequences. (a) Definition of tilt and kink angles. WT, A2T and D23N in (b), (c) and (d).

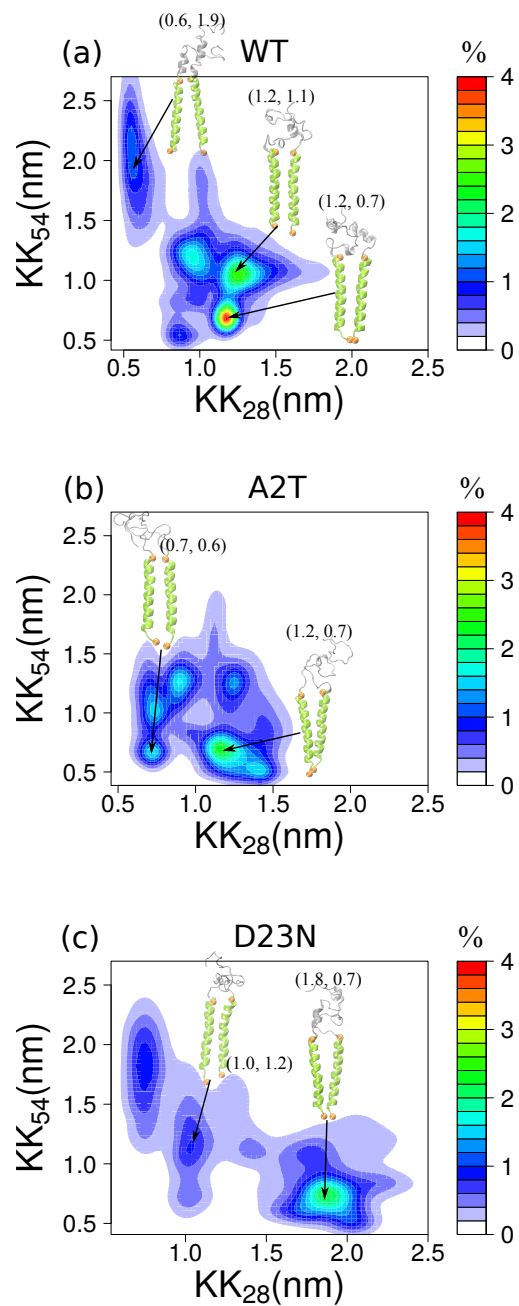


FIG. 6. Probability distance maps formed of $C\alpha$ K28A-K28B distances and $C\alpha$ K54A-K54B distances for WT (a), A2T (b) and D23N (c) respectively. Representative structures are shown in cartoon representation. The $C\alpha$ atoms of K28 and K54 are shown in orange spheres. Residues from 28 to 54 are shown in green, and residues 1 to 27 are shown in silver.

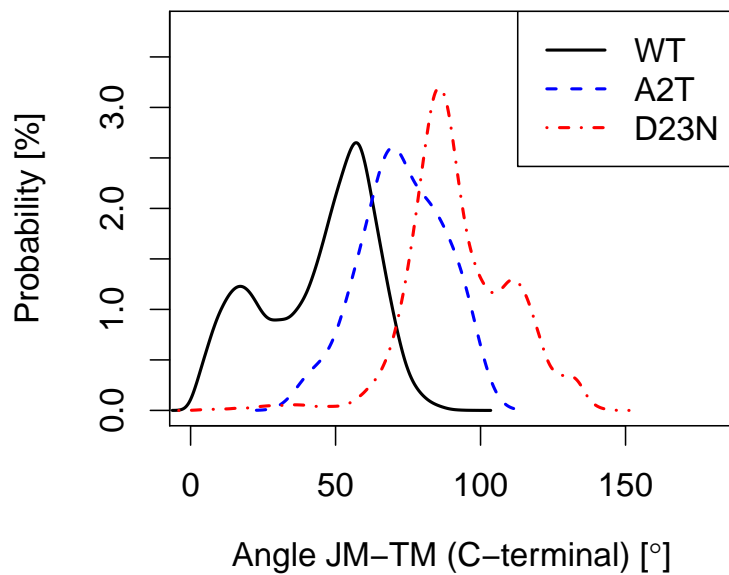


FIG. 7. Probability distribution of the crossing angle between the JM and the C-terminal TM helices for the three species.

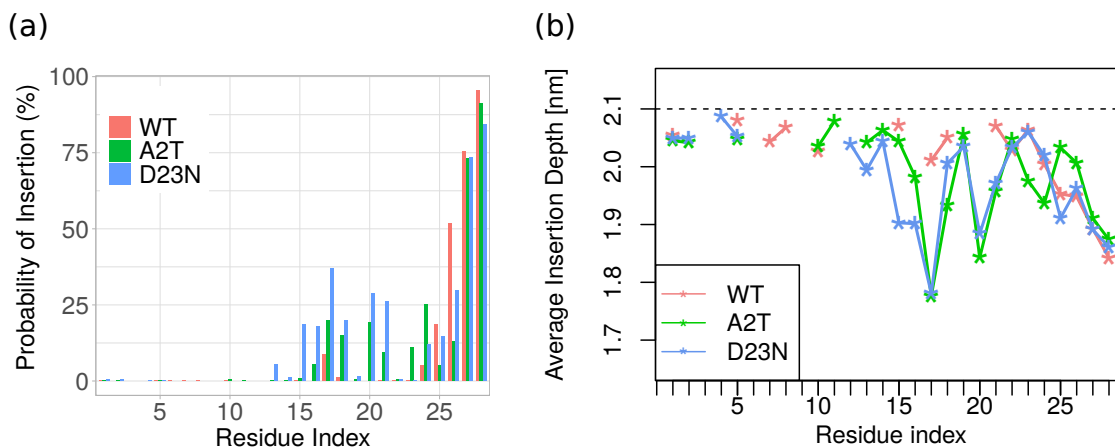


FIG. 8. (a) Probability of insertion of each residue into the lipid bilayer. (b) Average insertion depth of residues 1-28. One residue is considered as inserted into the membrane if the insertion depth is less than 2.1 nm. The insertion depth of each residue was calculated as the z component of the distance between the center of mass of each residue and the center of mass of all lipid P atoms of the membrane (the origin of the membrane). The upper-leaflet and lower-leaflet of P atoms locate at ± 2.1 nm. For clarity, we do not show the residues that are not inserted.

Supplementary Information for “Impact of A2T and D23N mutations on C99 homodimer conformations”

Yan Lu,¹ Freddie R. Salsbury Jr.,² and Philippe Derreumaux³

¹*School of Physics, Xidian University, Xi'an, 710071, China^{a)}*

²*Department of Physics, Wake Forest University, Winston-Salem, NC 27106, USA*

³*CNRS, Université Paris Cité, UPR 9080, Laboratoire de Biochimie Théorique, 13 rue Pierre et Marie Curie, Institut de Biologie Physico-Chimique, Fondation Edmond de Rothschild, 75005, Paris, France^{b)}*

Keywords: APP, C99, A2T and D23N mutations, Alzheimer’s disease, amyloid simulations

^{a)}Electronic mail: luyan@xidian.edu.cn

^{b)}Institut Universitaire de France (IUF), 75005, Paris, France; Electronic mail: philippe.derreumaux@ibpc.fr

Full T (%)	Coil	β -Sheet	β -Bridge	Bend	Turn	α -Helix	π -helix	3_{10} -helix
WT	36.2	4.0	0.9	13.7	16.6	23.3	0.0	5.2
A2T	43.9	1.7	2.9	23.6	15.7	6.2	0.0	5.8
D23N	35.3	1.7	0.9	17.6	18.8	19.4	0.3	5.9
First half T (%)	Coil	β -Sheet	β -Bridge	Bend	Turn	α -Helix	π -helix	3_{10} -helix
WT	34.2	3.1	0.6	14.1	17.4	24.2	0.0	6.3
A2T	43.7	0.1	2.8	22.6	17.1	7.8	0.0	5.8
D23N	36.0	1.9	1.0	17.7	17.4	19.6	0.1	6.1

TABLE S1. Secondary structure composition of the extracellular domain (residues 1-28) using the full trajectory of all simulations (Full T) and the first half trajectory of all simulations (First half T).

Full T (%)	Coil	β -Sheet	β -Bridge	Bend	Turn	α -Helix	π -helix	3_{10} -helix
WT	9.5	0.0	0.0	1.7	2.3	86.4	0.0	0.1
A2T	9.9	0.0	0.0	1.9	2.8	85.1	0.0	0.2
D23N	10.7	0.0	0.1	2.2	3.7	83.0	0.0	0.2
First Half T (%)	Coil	β -Sheet	β -Bridge	Bend	Turn	α -Helix	π -helix	3_{10} -helix
WT	9.5	0.0	0.0	1.5	2.0	86.9	0.0	0.1
A2T	10.5	0.0	0.1	2.1	2.7	84.4	0.0	0.2
D23N	10.6	0.0	0.0	2.1	3.6	83.4	0.0	0.2

TABLE S2. Secondary structure composition of the transmembrane domain (residues 29-52) and residues K53-K55 using the full trajectory (Full T) and the first half trajectory of all simulations (First half T).

WT	cluster 1	cluster 2	cluster 3	cluster 4	cluster 5
A2T 1	0.93	0.95	1.03	1.09	1.08
2	1.12	1.03	0.92	0.97	0.96
3	1.15	0.93	0.88	1.01	0.96
4	0.95	1.01	1.04	1.20	1.08
5	0.96	1.05	1.02	0.83	1.05
WT	cluster 1	cluster 2	cluster 3	cluster 4	cluster 5
D23N 1	0.60	0.75	0.80	0.88	0.87
2	0.66	0.98	1.02	1.00	1.11
3	1.09	0.98	0.77	0.95	0.98
4	0.60	0.87	0.97	0.94	0.99
5	0.65	0.94	0.92	0.92	1.05
A2T	cluster 1	cluster 2	cluster 3	cluster 4	cluster 5
D23N 1	0.82	1.01	1.09	1.03	0.85
2	1.09	1.21	1.26	1.08	0.98
3	0.99	0.83	0.94	1.07	1.04
4	1.02	1.13	1.16	1.04	0.94
5	1.11	1.06	1.11	1.09	0.99

TABLE S3. Cross $C\alpha$ RMSD (in nm) between the centers of the first five clusters of WT, D23 and A2T.

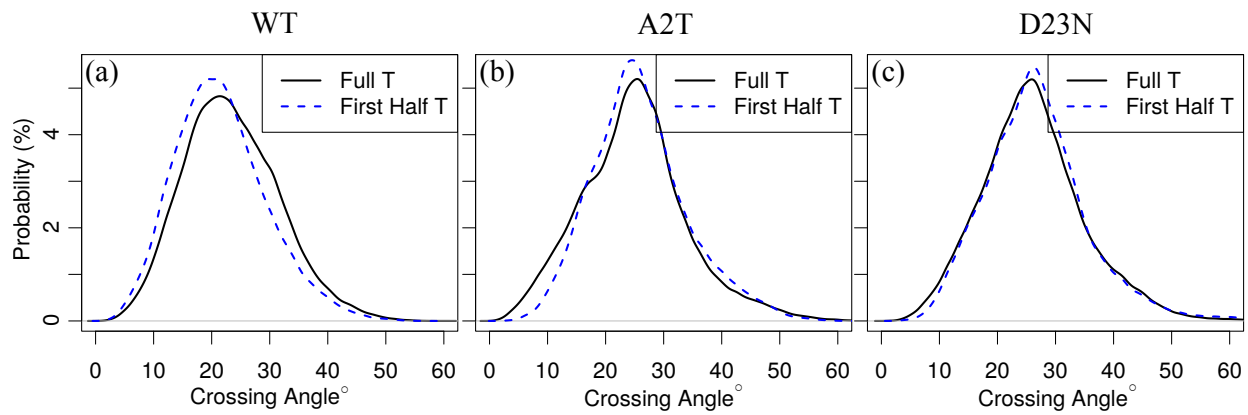


FIG. S1. Superposition of the probability distribution of the crossing angle in degrees between the two TM helices using the first half of all trajectories and the full length trajectories of each sequence.

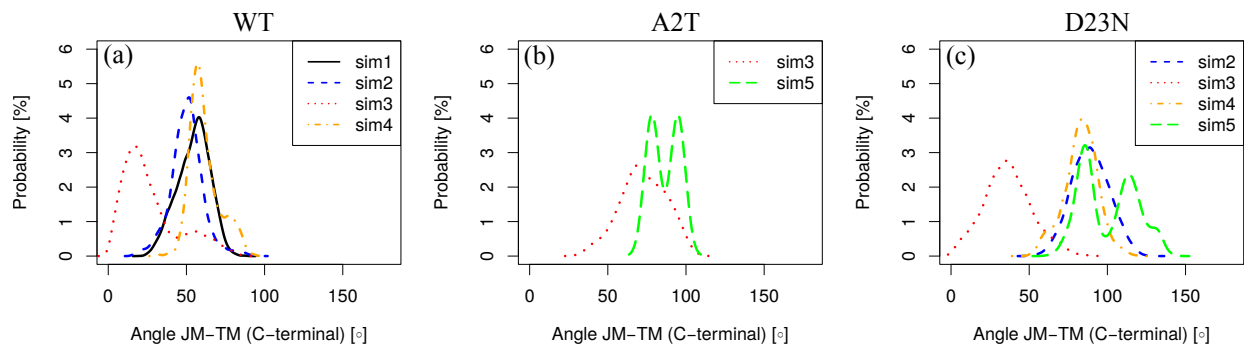


FIG. S2. Superposition of the probability distributions of the angle between the JM and the C-terminal TM helices using each of the five simulations of the three sequences. Note that there is no JM helix in simulation 5 of WT, no JM helix in simulations 1, 2 and 4 of A2T, and no JM helix in simulation 1 of D23N.

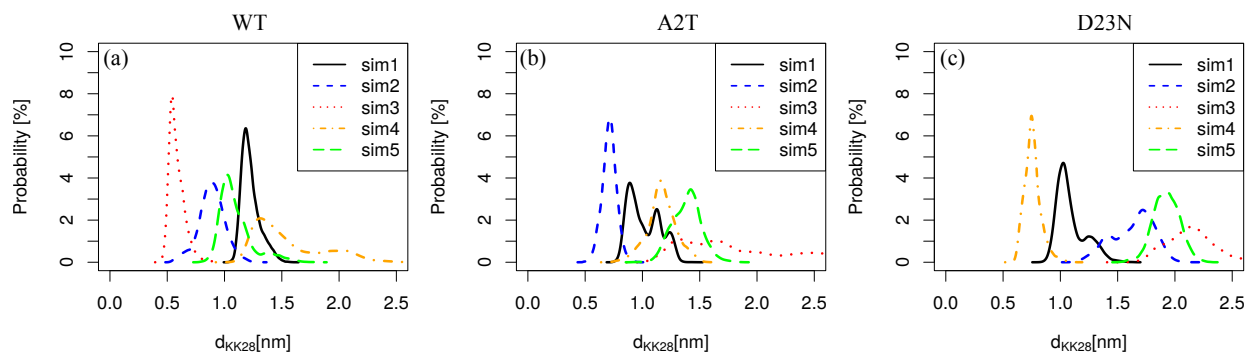


FIG. S3. Superposition of the probability distributions of the intermolecular C α K28K28 distances using each of the five simulations of the three sequences.

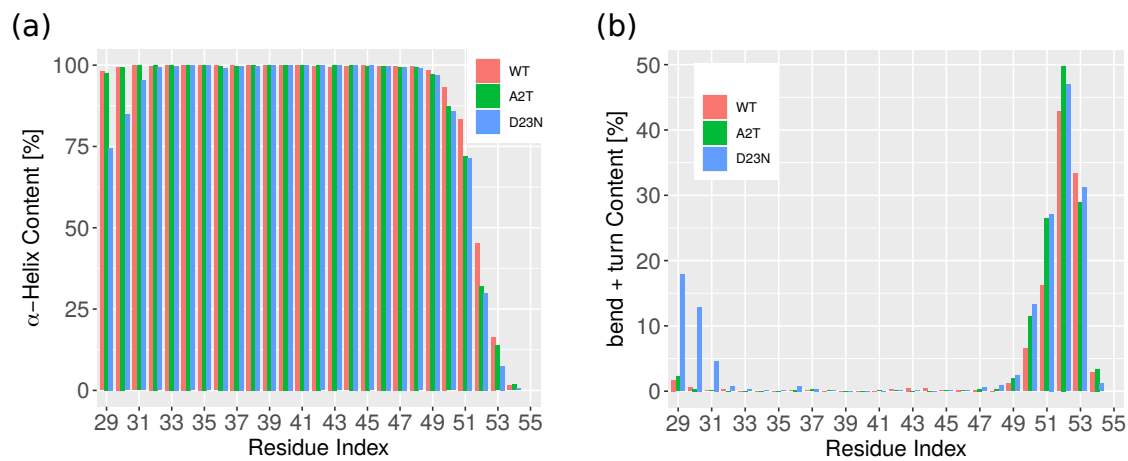


FIG. S4. Secondary structure content of the transmembrane domain (residues 29-52) and the K53-K55 amino acids. (a) α -helix, (b) turn+bend.

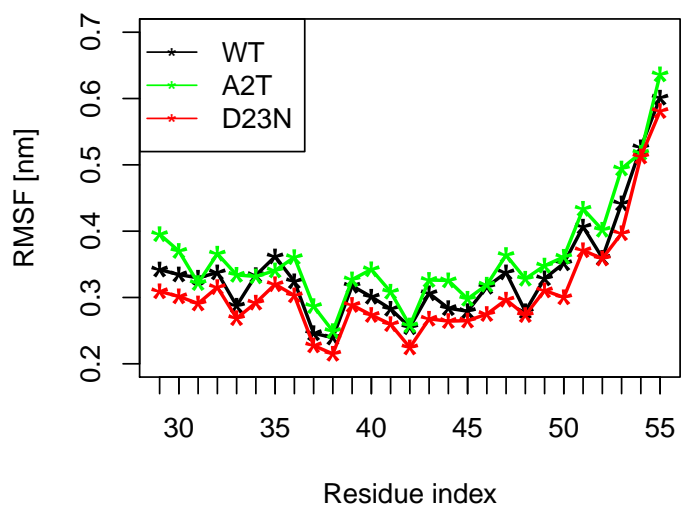


FIG. S5. Root-mean-square fluctuations (RMSF) of the transmembrane domain (residues 29-52) and the three residues K53-K55.

The **centers of** the first five clusters are shown in FIG. [S6](#). The cross RMSD values shown in Table S3 indicate large variability between the centers of the first five clusters of the WT, D23N and A2T sequences. The N-terminal region of A2T is mostly random coil with transient JM alpha-helices. Cluster 4 accounting for 4% of the full conformational ensemble displays an intermolecular beta-sheet spanning residues 18-20 and residues 21-23, and clusters 7 (3.1%), 9 (2.1%), and 10 (1.9%) display a parallel intermolecular beta-sheet spanning residues (15-17 and 12-14, 4-5 and 13-14, 18-20 and 21-23), respectively. The N-terminal region of D23N shows many transient JM helices, and a transient beta-hairpin spanning residues 5-6 and 11-12 (cluster 7, 2.1%). The N-terminal region of WT shows JM alpha-helix structures (clusters 1 and 4), and mixed alpha-beta structures with clusters 2 and 5 showing beta-hairpins spanning residues 4-7 and residues 10-13, and cluster 8 (1.9%) displaying a parallel intermolecular beta-sheet spanning residues 16-17 and 20-21.



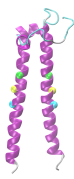












	cluster 1	cluster 2	cluster 3	cluster 4	cluster 5
WT	11.9% 	4.8% 	3.8% 	3.3% 	3.2% 
A2T	10.0% 	6.7% 	4.8% 	4.4% 	4.3% 
D23N	14.9% 	10.5% 	5.0% 	3.2% 	2.6% 

FIG. S6. Centers of the first five clusters of the full systems by using a C α RMSD cutoff of 3 Å. The percentages are shown on top of each snapshot. The peptides are shown in cartoon representation with α helix in purple, 3_{10} helix in blue, β content in yellow, turn in cyan, and coil in white. The C α atoms of G29, G33 and G37 are represented as green, yellow and cyan spheres respectively.

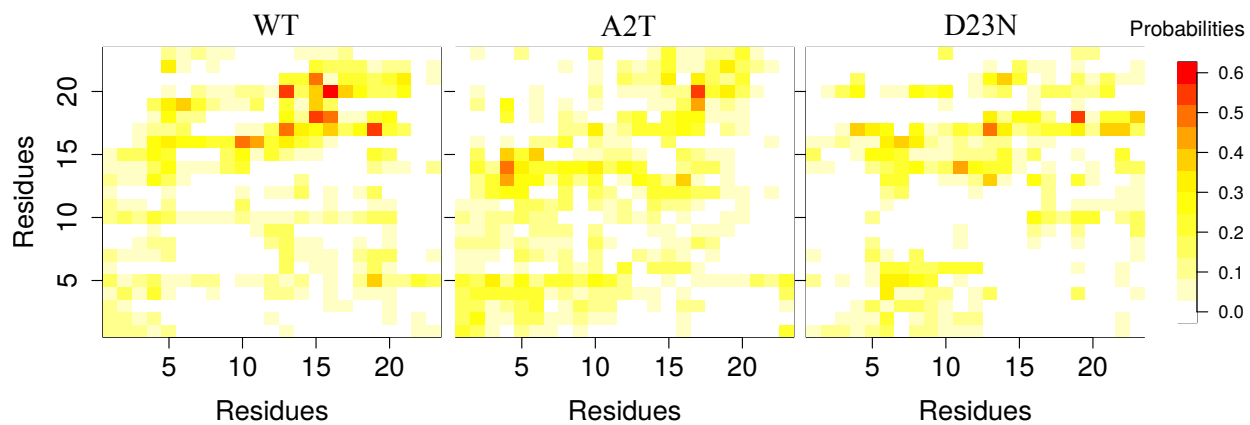


FIG. S7. The intermolecular side-chain side-chain contact probabilities of residues 1-23 for the three sequences. A contact is defined between two heavy atoms if the distance is less than 0.45 nm.